Macromolecules
ARTICLE

Macromolecules **2009**, *42*, 8411–8422 **8411**
DOI: 10.1021/ma9015449

Internal Structure of Ultrathin Diblock Copolymer Brushes

Bulent Akgun,[†,‡,§] Gökçe Uğur,[†] William J. Brittain,[†] Charles F. Majkrzak,[‡] Xuefa Li,[⊥] Jin Wang,[⊥] Huimin Li,[∥] David T. Wu,[∥] Qiang Wang,[#] and Mark D. Foster*[,†]

[†]*Department of Polymer Science, The University of Akron, 170 University Avenue, Akron, Ohio 44325-3909,* [‡]*NIST Center for Neutron Research, National Institute of Standards and Technology, Gaithersburg, Maryland 20899,* [§]*Department of Materials Science and Engineering, University of Maryland, College Park, Maryland 20742,* [⊥]*X-ray Science Division, Argonne National Laboratory, Argonne, Illinois 60439,* [∥]*Chemical Engineering and Chemistry Departments, Colorado School of Mines, Golden, Colorado 80401, and* [#]*Department of Chemical and Biological Engineering, Colorado State University, Fort Collins, Colorado 80523*

Received July 15, 2009; Revised Manuscript Received August 31, 2009

ABSTRACT: The internal structure of as-deposited, high grafting density, ultrathin (thickness < 25 nm) diblock copolymer brushes (DCBs) is resolved using neutron reflectivity (NR) and grazing incidence small-angle X-ray scattering (GISAXS). DCBs of various thicknesses containing deuterated polystyrene (dPS) blocks and poly(methyl acrylate) (PMA) blocks with dPS (dPS-*b*-PMA) or with PMA (PMA-*b*-dPS) adjacent to the substrate were synthesized by atom transfer radical polymerization (ATRP). For the thinnest films, a model of two layers with a smooth interfacial gradient provides a good description of the data. For thicker dPS-*b*-PMA samples of sufficiently asymmetric composition, a third layer must be included. This is consistent with the presence of lateral ordering in the center of the brush, as evidenced by GISAXS data. For the thinnest DCBs, the gradient in composition perpendicular to the surface extends through nearly the entire thickness of the brush, consistent with the conjecture that the gradient is imposed by the presence of the surface field and tethering on a material that, in the absence of tethering, would be disordered. The interface widths for brushes with a PMA block tethered to the substrate are smaller than for brushes with a dPS block tethered to the substrate. In general, the region adjacent to the substrate is found to have a substantial composition of the "top" block in contrast to expectations from theory. Experimental interface width values are consistent with expectations from self-consistent field theory for brushes with a dPS bottom block. A scaling theory for the interfacial width in a DCB identifies a crossover as $(d/R_g)^2 > \chi N$ from the classical Helfand−Tagami regime, where $w \approx b/(\chi^{1/2})$, to a new *stretched interface* regime, where $w \approx d/(\chi N)$. The scaling theory provides insight into how interface width in the DCBs should vary with grafting density, interaction parameter, and chain molecular weight and is qualitatively consistent with the experimental data and suggests directions for further work.

Introduction

Diblock copolymer brushes (DCBs) have garnered enormous interest recently due to the observation that their surface character can be substantially altered by treatment with a solvent selective for one of their blocks.[1] This means they may be used as stimuli responsive materials in sensors, biomimetics, or microfluidics. Zhao et al.[1a] showed for the first time, using contact angle measurements and atomic force microscopy (AFM), that the surface of a polystyrene-*b*-poly(methyl methacrylate) (PS-*b*-PMMA) brush can be rearranged by changing the character of the solvent contacting the brush before it is dried. In their study, the advancing water contact angle of the surface of a PS-*b*-PMMA DCB (with the first block noted being that next to the substrate) was changed from that characteristic of PMMA to that characteristic of PS by changing the solvent from dichloromethane, a good solvent for both polymers, to cyclohexane, a good solvent at 35 °C for the PS block ($M_n \approx 30$ kg/mol) and a poor solvent for the PMMA block. They also demonstrated, using intermittent-contact mode AFM imaging, that the surface morphology changed after selective solvent treatment, forming a nanopattern at the surface.

*To whom all correspondence should be addressed. E-mail: mfoster@uakron.edu.

After this paper, the surface rearrangement of diblock[1,2] and triblock[3] copolymer brushes was studied by various authors using contact angle measurements, AFM, X-ray photoelectron spectroscopy (XPS), ATR-IR, and ellipsometry. Most of these studies demonstrated that surface rearrangement could be observed with a variety of block combinations in various solvents, but none of them explained how the surface rearrangement happens. Zhao and co-workers[1a] conjectured what the internal structures of the brush films might be in the as-deposited and "switched" states, but they did not confirm the internal structure since it could not be resolved with their techniques. To date, neither the "as-deposited" structure nor the switched structure has been established. The mechanism of the surface rearrangement remains to be elucidated as well. Clarifying the structures of the as-deposited and switched states is the first step to understanding and controlling surface rearrangement.

There have been self-consistent field (SCF) theoretical studies[4] of what to expect for equilibrium "wet" DCBs when it can be assumed that the composition varies only in the direction perpendicular to the substrate. There have also been 2D SCF[5,6] and Monte Carlo[4a] simulations for wet DCBs in which composition varies in the directions both parallel and perpendicular to the substrate. These studies predict very rich phase behavior for DCBs in solvent, with the predicted morphology depending on

Published on Web 09/23/2009

the volume fraction (f) of one block, Flory−Huggins exchange interaction parameter (χ) between solvent and polymers, and molecular weight or length (N) of the chains. Two studies[7,8] have focused on DCBs in the melt state. Heine and Wu[8] pointed out that the interface between the A-rich and B-rich domains will be sharper when the DCB is "dry". In this paper, we present first experimental results elucidating the internal structure of dry, "as-deposited" ultrathin DCBs using neutron reflectivity (NR).

Neutron reflectometry (NR) is a powerful technique for characterizing thin film structure in the direction perpendicular to the surface.[9] In reflectometry, the ratio of specularly reflected intensity to incident intensity is measured for a thin film over a range of incident angles (θ) to yield a reflectivity curve. Information about the film thickness, microroughnesses at the substrate/film and air/film surface and neutron scattering length density (SLD) profile can be obtained from the reflectivity curve. NR is the superior nondestructive technique for the investigation of interfacial structures "buried" inside the film due to the larger contrast that can be obtained through selective deuteration. The depth resolution of film structure with NR is on the order of 1 nm and is dependent on the range of scattering vector $\mathbf{q}$ ($|\mathbf{q}| = 4\pi \sin\theta/\lambda$) over which data are collected. Because the neutron scattering lengths of the isotopes hydrogen and deuterium differ tremendously, deuteration of one block in a DCB enhances the neutron scattering contrast between domains rich in differing blocks and makes the interfacial region visible to neutrons in a way not generally possible with X-rays.

Experimental Section

DCBs containing deuterated polystyrene (dPS) blocks were synthesized for NR measurements. Because NR measurements require substrates at least 6 cm in one dimension, the polymerizations were performed in a drybox instead of a Schlenk flask. The polymerization procedure was therefore modified from that for typical synthesis of a PS-*b*-PMA brush.[3a]

Materials. Deuterated styrene (S-d_8; C/D/N Isotopes or Cambridge Isotope Laboratories, 98% by atom)[10] and methyl acrylate (MA, Aldrich, 99%)[10] were passed through a column of activated basic alumina and degassed with high purity nitrogen for 1 h prior to use. CuBr (Aldrich, 98%)[10] was purified as described in the literature.[11] *N*,*N*,*N*′,*N*″,*N*″-Pentamethyldiethylenetriamine (PMDETA, Aldrich, 99%),[10] ethyl 2-bromoisobutyrate (E2Br-iB, Aldrich, 98%)[10] and anhydrous anisole (Aldrich)[10] were used as received. Silicon ATR crystals ($25 \times 5 \times 1$ mm) were obtained from Harrick Scientific.[10] Silicon wafers (100) doped with phosphorus having 500 ± 50 μm thicknesses were purchased from Umicore Semiconductor Processing.[10] All other reagents were purchased from Aldrich or Fisher Scientific and used as received.

Substrate Preparation. ATR crystals and silicon wafers ($60 \times 35 \times 0.5$ mm) were cleaned by treatment with a freshly prepared "piranha" solution[12] (70/30, v/v, concentrated H_2SO_4/30% aqueous H_2O_2) between 90 and 100 °C for 2 h and were then rinsed with distilled water and dried with a stream of compressed air.

General Procedure for Deposition of Surface Bound Initiator. A 100×50 mm^2 crystallizing dish was placed in a drybox, and a freshly cleaned silicon wafer and ATR crystal were placed in the crystallizing dish. The (11-(2-bromo-2-ethyl)propionyloxy)undecyltrichlorosilane was synthesized according to the literature[13] and utilized as a surface-bound initiator. Dry toluene (30 mL) and a 25 vol % solution of the trichlorosilane initiator in toluene (0.6 mL) were added to the dish via syringe, and the dish was covered with a piece of glass carrying a Teflon gasket and heated at 60 °C for 4 h in the drybox. The silicon wafer and ATR crystal were then removed, sequentially washed with toluene, ethanol, and methylene chloride, and then dried in a stream of compressed air.

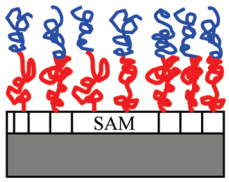

Figure 1. Idealized schematic of an **ideal** DCB with a very sharp interface between the two lamellar domains, each rich in a particular block.

Procedure for Surface ATRP from a Flat Silicon Substrate. CuBr, anisole, and monomer were added to a 100 mL Schlenk flask with a magnetic stir bar, sealed with a rubber septum, and degassed by purging with technical grade nitrogen for 2 h. Three vacuum/purge cycles were applied to the flask and it was left under a nitrogen atmosphere. PMDETA was added to the mixture via syringe and the solution was stirred at reaction temperature until it became homogeneous (≈5 min). Then the flask was sealed and transferred to the drybox along with the free initiator (ethyl-2-bromoisobutyrate, E2Br-iB), ATR crystal, silicon wafer, and a 100×50 mm^2 crystallizing dish. An initiator-modified ATR crystal and silicon wafer were placed in the crystallizing dish in the drybox. Polymerization solution was added to the crystallizing dish, followed by the addition of free initiator. The final concentrations were as follows: $[\text{S-}d_8]_0$ = 3.9 M, $[\text{PMDETA}]_0$ = 25 mM, $[\text{CuBr}]_0$ = 12 mM, and $[\text{Br-iB}]_0$ = 5 mM or $[\text{MA}]_0$ = 3.7 M, $[\text{PMDETA}]_0$ = 30 mM, $[\text{CuBr}]_0$ = 15 mM, and $[\text{Br-iB}]_0$ = 15 mM. The dish was covered with a piece of glass carrying a Teflon gasket to prevent evaporation of the solution. The polymerization proceeded at 90−100 °C for a period of time, depending on the thickness targeted, after which the ATR crystal and silicon wafer were removed. To remove untethered polymer chains, the ATR crystal and silicon wafer were placed in a Soxhlet extractor and extracted with tetrahydrofuran (THF) for 24 h, followed by sonication in THF for 30 min.

Block Copolymerizations. To create a block copolymer brush, a second block was polymerized by ATRP in the same manner as the S-d_8 or the MA homopolymer layers were polymerized. For example, the dPS-*b*-PMA brush was produced by first polymerizing the dPS block using S-d_8 and then polymerizing the PMA block using methyl acrylate from dPS macroinitiator. After each polymerization, the ATR crystal and silicon wafer were cleaned and extracted to remove any untethered polymer before proceeding to the next polymerization. Figure 1 shows an idealized DCB structure. It has been assumed by a majority of papers in the literature that an "as-deposited" DCB has a lamellar structure with a layer rich in the first block synthesized next to the substrate and a layer rich in the other block adjacent to the air surface. Most of the schematic drawings in brush papers have also shown a sharp interface between domains rich in different blocks.

Throughout this paper, DCBs will be identified using the thickness of the layer of the polymer created when a particular block was synthesized, with these thicknesses measured with ellipsometry or calculated from NR results. For example, the sample designation "dPS14-PMA3" indicates that a 14 nm thick dPS layer was first synthesized on top of the initiator layer, and when the PMA block was synthesized, the overall thickness of the dry brush increased by 3 nm.

Characterization Methods. FTIR-ATR spectra were recorded using a Nicolet System 730 spectrometer with a modified 4XF beam condenser (Harrick Scientific).[10] Spectra were recorded at 2 cm^{-1} resolution, and 500 scans were collected. Contact angles were determined using a Rame Hart NRL-100 goniometer[10] equipped with a tilting base mounted on a vibrationless table. Advancing and receding contact angles of a 10 μL drop were determined using the tilting stage method. Ellipsometry measurements were performed on a Gaertner model L116C ellipsometer[10] with a He−Ne laser (λ = 632.8 nm) and a fixed angle of

Table 1. Physical Properties of Samples for PMA-*b*-dPS Series

sample	$M_{n,PMA}$[a] (kg/mol)	$M_{n,dPS}$[a] (kg/mol)	N_{PMA}	N_{dPS}	d_{PMA}[b] (nm)	d_{dPS}[b] (nm)	χN
PMA2-dPS4	1.8	5.7	21	51	2	4	7.2
PMA6-dPS5	4.8	5.7	55	51	6	5	10.6
PMA7-dPS2	4.8	3.2	55	29	7	2	8.4
PMA8-dPS2	6.6	3.2	76	29	8	2	10.5

[a] Number averaged molecular weights were measured using gel permeation chromatography (GPC) for free chains in solution created at the same time the brush was synthesized. [b] Thickness (d) values are from NR.

Table 2. Physical Properties of Samples for dPS-*b*-PMA Series

sample	$M_{n,dPS}$[a] (kg/mol)	$M_{n,PMA}$[a] (kg/mol)	N_{dPS}	N_{PMA}	d_{dPS}[b] (nm)	d_{PMA}[b] (nm)	χN
dPS5-PMA2	5.1	3.9	49	46	5	2	9.5
dPS14-PMA3	14.5	5.7	139	66	14	3	20.5
dPS15-PMA4	14.5	8.6	139	100	15	4	23.9
dPS15-PMA6	19. 6	8.2	188	95	15	6	28.3
dPS11-PMA8	11.7	11.1	104	130	11	8	23.4
dPS14-PMA9	19.9	12.8	191	152	14	9	34.3

[a] Number averaged molecular weights were measured using GPC for free chains in solution created at the same time the brush was synthesized. [b] Thickness (d) values are from NR for the first two samples. The rest are from ellipsometry measurements.

incidence of 70°. For the layer thickness calculations, the following refractive indices were used: 1.455 for silicon oxide, 1.508 for initiator layer, 1.589 for PS, and 1.48 for PMA.

Brush internal structure was characterized using NR and grazing incidence small-angle X-ray scattering (GISAXS).[14] In GISAXS measurements, a fixed glancing incident angle is used, and scattering for a range of both q_z and q_y are collected using a two-dimensional image plate detector. Such measurements provide information on nonlamellar structure internal to the brush and, particularly, on lateral correlations in the plane of the brush. GISAXS experiments were carried out at the 8-ID-E beamline at the Advanced Photon Source using a monochromatic X-ray beam with a wavelength of 0.1675 nm. The beam quality was optimized using a setup of high-quality entrance slits and a completely evacuated pathway. The beam had a vertical size of 50 μm and a horizontal size of 150 μm. The sample-to-detector distance was 1.975 m. The scattered intensity was recorded at a fixed angle of incidence, α_i, of the X-ray beam onto the sample surface using a two-dimensional image plate detector with 150 μm pixel size and 1200 × 1200 pixel array.

NR measurements were performed on the NG1 vertical reflectometer at the National Institute of Standards and Technology (NIST) Center for Neutron Research using a wavelength of 0.475 nm. To maximize the intensity, the sizes of the collimating slits and detector slits were increased during the measurement as incident angle (θ) increased, keeping the relative resolution in q approximately constant ($\delta q/q \approx 0.02$). Data were corrected for both the varying slit size and background. To reduce background scattering, all measurements were done with the sample in an aluminum sample chamber evacuated by a turbomolecular pump.

The structure of thin films cannot be obtained directly by inverting the reflectivity data due to loss of phase information.[9a,15,16] Instead, a candidate model is assumed for the thin film structure and the parameters of the model are varied using a nonlinear regression until a simulated reflectivity curve calculated for the model structure using the Parratt formalism[17] agrees sufficiently well with the experimental data. In the Parratt formalism, the reflectivity of the whole sample is found by calculating the reflectivity for the substrate/sample interface and then solving recursively for the reflectivity for each subsequent interface as one proceeds to the sample/air interface. If enough is known about the film's composition and structure from its preparation or other techniques, this indirect analysis is very powerful, providing film thicknesses and interface widths with great precision. It is not a unique solution, but other reasonable models can be tried and excluded.

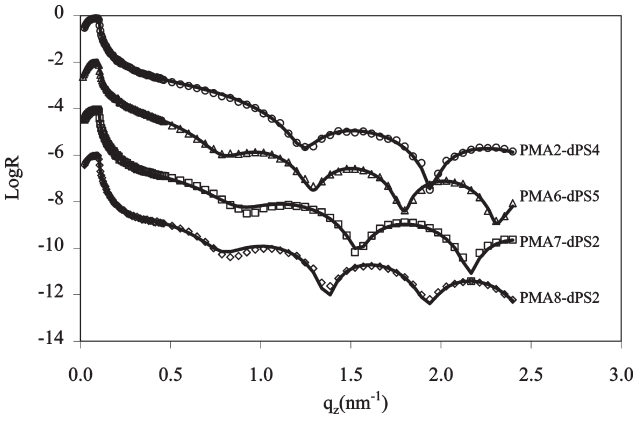

Figure 2. The neutron specular reflectivity (open symbols) and best fit model curve are plotted as a function of wavevector in the direction normal to surface, q_z, for a series of PMA-*b*-dPS brushes. Adjacent curves have been shifted vertically by 2 orders of magnitude for clarity. Error bars are smaller than the data symbols in all reflectivity plots and they represent ±1 "standard deviation".

Results and Discussion

Solution deposition of the initiator onto silicon substrate and ATRP of dPS and PMA on the surface was confirmed using ATR-IR, contact angle measurements, and ellipsometry (see Supporting Information). The specific conditions for ATRP of dPS and PMA were given in the Experimental Section. PMDETA was chosen as ligand for all ATRP reactions due to increased catalyst complex solubility of the multidentate amine ligands when employing copper metal (CuBr) as the ATRP catalyst.[18] It has been shown that the low concentration of initiator on flat surfaces causes an insufficient concentration of the deactivator to provide control during the surface ATRP reactions.[19] To overcome this problem, free initiator (E2Br-iB) was added to the reaction solution. The other advantage of using free initiator is that the free polymer grown in solution can be used to characterize the molecular weight and polydispersity of the grafted chains, because the amount of tethered polymer on the silicon wafer is too small to degraft and analyze. The validity of equating the molecular weight of the free polymer in solution and that on the surface has been tested by various groups for ATRP[19] and other controlled radical polymerization techniques.[2d,20] The physical properties of the PMA-*b*-dPS and dPS-*b*-PMA samples are shown in Tables 1 and 2, respectively.

Table 3. Calculated[a] and Experimentally Measured[b] Solubility Parameters

monomer	calculated[a] δ (J/cm^3)$^{1/2}$	experimental[b] δ (J/cm^3)$^{1/2}$
methyl acrylate	19.9	19.9−21.3
styrene	19.1	17.4−19.0
methyl methacrylate	19.0	18.8−26.2
isoprene	17.4	16.2−20.5

[a] Calculated using the method of Hoftyzer and van Krevelen.[21] [b] Values taken from ref 21.

Structure of DCBs with PMA on the Bottom. Figure 2 shows the neutron reflectivity as a function of scattering vector normal to surface, q_z, for all samples from the PMA-*b*-dPS series. The fits were obtained using a model of the brush structure consisting of a bottom layer of one SLD, a top layer of a second SLD, and an interface between the layers created by convoluting the step change in SLD between layers with a Gaussian of appropriate width. Roughnesses at the other interfaces were modeled by convolution with appropriate Gaussian functions as well. In other words, a purely lamellar structure model was used. The reflectivity curves have been measured up to a q_z value of 2.4 nm^{-1} to resolve the smaller scale details of the interface structure. For all these films, such a model captures all the features of the reflectivity curves, even though most of the films have asymmetric composition. This suggests that the effective fields resulting from tethering to the substrate, the affinity of PMA for the substrate, and the affinity of dPS for the air surface serve to force these brushes to form lamellar structures, even though equivalent, untethered diblock molecules might not do so in a bulk melt.

The fact that for thin brushes for which N is low and therefore the value of the combination parameter χN is low order into lamellar structures, even for asymmetric compositions, suggests that low value of χN may be the key characteristic in determining the type of structure formed. The parameter χN is a key parameter in characterizing the tendency of untethered block copolymer chains to microphase segregate in the bulk. For large values of N, block copolymer chains of near symmetric composition order in the bulk for values of χN of order 10. Due to the influence of composition fluctuations, the value of χN above which ordering occurs $(\chi N)_{\text{disorder-order}}$, is even larger for smaller values of N for which fluctuations become important. The value of $(\chi N)_{\text{disorder-order}}$ also increases as one moves away from symmetric composition. Because the PS-*b*-PMA block copolymer has not been widely studied, there is no published value of χ. For making rough comparisons to the behavior expected in the bulk, we have thus estimated the value of χ from solubility parameter arguments. At this level of approximation, the exchange interaction parameter χ_{AB} is given by

$$\chi_{AB} = \frac{V_r}{RT}(\delta_A - \delta_B)^2 \quad (1)$$

where δ_i is the solubility parameter of species i, V_r is the reference volume of a polymer segment, and R is the universal gas constant. Values calculated for PS and PMA using a group additivity calculation, as described by van Krevelen,[21] are compared in Table 3 with experimental values from the literature and values for two other polymers, poly(methyl methacrylate) (PMMA) and polyisoprene (PI), for which the interaction parameter with PS has been measured experimentally.

Rather than estimating the value of $\chi_{PS\text{-}b\text{-}PMA}$, simply using eq 1, we take into account published values of $\chi_{PS\text{-}b\text{-}PMMA}$ and $\chi_{PS\text{-}b\text{-}PI}$, which should bound the value of $\chi_{PS\text{-}b\text{-}PMA}$. In a small-angle neutron scattering study[22] of disordered dPS-*b*-PMMA, the value of $\chi_{PS\text{-}b\text{-}PMMA}$ was determined as 0.041 at 298 K. The value of $\chi_{PS\text{-}b\text{-}PI}$ was measured by small-angle X-ray scattering as 0.14 at 298 K.[23] Using a constant reference segment volume for all values of χ, we can estimate ratios of the relative magnitudes of $\chi_{PS\text{-}b\text{-}PMA}$, $\chi_{PS\text{-}b\text{-}PMMA}$, and $\chi_{PS\text{-}b\text{-}PI}$.

$$\chi_{PS\text{-}b\text{-}PMA}/\chi_{PS\text{-}b\text{-}PMMA} = (\delta_{PS} - \delta_{PMA})^2/(\delta_{PS} - \delta_{PMMA})^2 = 64 \quad (2)$$

$$\chi_{PS\text{-}b\text{-}PMA}/\chi_{PS\text{-}b\text{-}PI} = (\delta_{PS} - \delta_{PMA})^2/(\delta_{PS} - \delta_{PI})^2 = 0.22 \quad (3)$$

We thus expect that a good estimate of $\chi_{PS\text{-}b\text{-}PMA}$ should be considerably larger than the value of $\chi_{PS\text{-}b\text{-}PMMA}$ (0.04) and somewhat smaller than that for $\chi_{PS\text{-}b\text{-}PI}$ (0.14). We choose a value of 0.1 for $\chi_{PS\text{-}b\text{-}PMA}$ because it lies between these experimentally known bounds even though it does not satisfy either eq 2 or 3.

Estimates of χN are included in Tables 1 and 2. One sees that the value of χN for the thinnest sample is sufficiently low that it is unlikely that untethered chains of this composition and length would microphase segregate in the bulk. To confirm that the layered structure is the right model for the samples with low χN values, an attempt was made to fit the data using a model of a single layer of uniform SLD, which is the average of the SLDs of the two blocks. The data could not be fit with this model even for the sample, which has the lowest χN value. The separation of PMA and PS segments observed for this sample is due to the effective fields acting on the chains as a result of the tethering and preference of dPS for the surface due to its smaller surface energy. The scattering length density profile for sample PMA6-dPS5, shown in Figure 3, has well-defined bottom and top layers. The value of χN for this sample is markedly higher and the biasing is sufficient to yield a well-defined interface between microphase segregated regions.

That the structure is indeed lamellar may be checked using 2D GISAXS measurements, which are sensitive to variations in structure in the plane of the sample. The 2D GISAXS

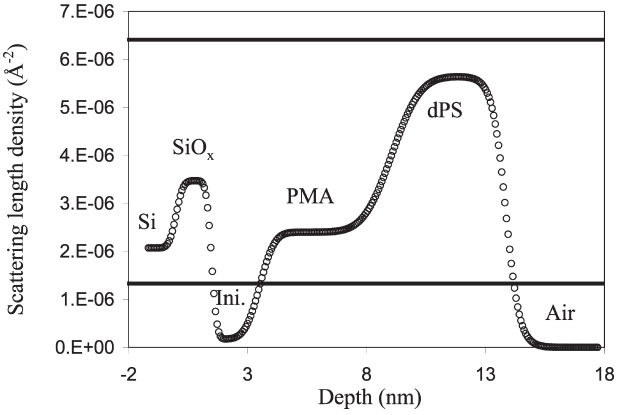

Figure 3. Scattering length density as a function of depth for the PMA6-*b*-dPS5 sample. The text markings on the plot approximately identify the material to which that portion of the SLD profile corresponds. For example "dPS" refers to that part of the sample that is rich in dPS, not necessarily pure dPS. The upper bold line represents the calculated SLD value expected for bulk, pure dPS ($b/V = 6.48 \times 10^{-6}$ Å^{-2}) and the lower bold line is that for bulk, pure PMA ($b/V = 1.26 \times 10^{-6}$ Å^{-2}).

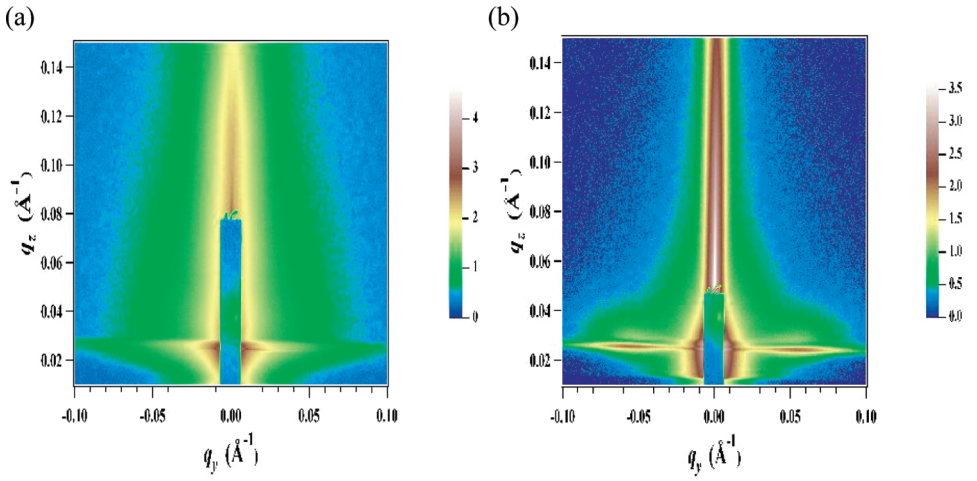

Figure 4. GISAXS data for PMA8-dPS2 (a) and of a PMA-*b*-PS (b) DCBs. PMA-*b*-PS has longer blocks. Intensity is plotted in false color as a function of α_f (incident angle) and $2\theta_f$.

pattern for the PMA8-dPS2 sample shown in Figure 4a contains no remarkable scattering features to the left or right of the plane of incidence, which intersects the detector at the center of the image. This indicates that the structure of the PMA8-dPS2 brush is uniform along the y direction in the plane of the sample, even though it has a highly asymmetric composition. For the same diblock copolymer in bulk, one would expect to find dPS-rich spheres or cylinders in a PMA-rich matrix, since the volume fraction of dPS is 0.28. The GISAXS data pattern shown in Figure 4b belongs to a thicker sample and shows scattering peaks to the left and right of the center. These indicate the presence of an in-plane liquid-like structure which will be discussed further in a future publication.

The stabilization of a lamellar structure is also favored by the presence of van der Waals interactions between the substrate and the polymeric layers, which serve to suppress fluctuations in the surface and in the interface between lamellar layers.[24] The very smooth surfaces seen for the PMA-*b*-dPS samples are consistent with the presence of such a suppression of fluctuations, though further proof of the fluctuation suppression is the subject of a separate publication.[25] The root-mean-square roughness (σ_{rms}) at the air surface for this series varies from 0.3 to 0.6 nm. We have reported in a previous paper[26] that the roughnesses of the air and substrate interfaces of thin dPS-*b*-PMA diblock copolymer brushes are correlated. The PMA-*b*-dPS samples in this work exhibit the same conformal roughness behavior.

We may also make some additional observations on the structure of the brushes on the basis of details of the model. We have elaborated our model to the extent that we have considered explicitly both the SiO_x on the substrate and the initiator layers. The thickness of the oxide layer was 1.2 ± 0.2 nm (uncertainties represent $\pm$ 1 "standard deviation"), and the thickness of the initiator layer varied from 1.3 to 2 nm. The thickness of the initiator layer expected from a calculation based on the chemical structure was 2.1 nm, whereas XR measurements done on a sample consisting of only an initiator layer on a substrate yielded an experimental thickness of 1.9 nm. When the thickness of the initiator layer in the model is lower than 1.9 nm, this may indicate that the grafting density of the initiator layer is lower than the maximum possible, and therefore, the layer is not close packed. The presence of a loosely packed initiator layer should not affect the final properties of the brushes significantly, so long as the density of initiator sites is still large enough that it substantially exceeds the grafting density of the polymer chains.

The values of SLD observed in each of the polymer-rich layers yield valuable quantitative information about the brush structure. The SLD is shown in Figure 3 as a function of depth for the lamellar model of sample PMA6-dPS5. The upper bold line in Figure 3 marks the value of SLD calculated for pure dPS at a density characteristic of a bulk melt (1.14 g/cm^3) and the lower bold line represents the value of SLD calculated for pure, bulk PMA melt (1.15 g/cm^3). The best fit model involves a value of SLD for the dPS-rich layer that is lower than the SLD for pure dPS. It also includes a value of SLD for the PMA-rich layer that is higher than the SLD value for pure PMA at bulk density. There are four possible explanations for this behavior. First, there could be substantial mixing of the two types of blocks in both layers. Second, the density of the brush might be markedly less than that of the corresponding polymers in the bulk. This seems unlikely and does not explain the high SLD of the PMA-rich layer. Third, it is possible that when the second block was synthesized, reaction initiated not only at the end of the first blocks, but also at some sites remaining on the surface of the substrate because only 10% of the initiator molecules initiate the polymerization at the first polymerization step.[27,28] Finally, only 85−90% of the homopolymers reinitiate to yield block copolymer.[3b] Thus, our DCBs contain approximately 10% homopolymer brush of the "bottom" block.

For ready comparison with theoretical calculations, it is convenient to focus specifically on a measure of the width of the interface between the two layers. To calculate the interface width, the SLD profile was first converted to a profile of volume fraction of dPS or PMA. It is not possible to calculate volume fractions unambiguously for the whole SLD profile because, very close to the substrate, there is a mixing of the SLDs of three components: the initiator, the PMA, and the dPS segments. In those locations there are two independent variables and one equation to solve. The same problem exists near the air surface where the model SLD contains contributions from the air, the dPS segments, and the PMA segments. The composition profile in the neighborhood of the interface between the two polymer layers for PMA6-dPS5 is shown in Figure 5. There are substantial fractions of dPS segments in the PMA-rich layer and PMA segments in the dPS-rich layer. The interfacial width is calculated using Helfand's[29] convention. A tangent to the composition profile is drawn at the depth at which the composition lies

halfway between its values in the two layers and extended to intersect horizontal lines corresponding to the compositions of the two layers. The projection of the distance between these intersections onto the depth axis is the interface width w. In our SLD model, the width at the interface between PMA-rich and dPS-rich layers is expressed using an error function. The value of full width at half-maximum (σ_{fwhm}) for the error function provides another measure of interface width. The value of w may be calculated by multiplying σ_{rms} by $(2\pi)^{1/2}$ to get σ_{fwhm}. The interface width calculated using Helfand's convention and calculated from the latter method are almost identical. The experimental interface width, w_{exp}, between the polymer domains varies from 2 to 3.3 nm for the PMA-*b*-dPS series (Table 4). Even though the calculated interface width is not large compared to the values obtained for untethered chains of PS-*b*-PMMA,[9b] when the total film thickness is taken into consideration, the interfacial region constitutes 25−30% of a film's volume.

Structure of DCBs with dPS on the Bottom. Changing the sequence in which the blocks are synthesized changes the balance among the different forces dictating the interface structure. PMA has a slightly higher surface energy (41.8 dyn/cm at 293 K)[30] than does the dPS (40 dyn/cm at 293 K),[30] and it has a higher affinity for the substrate. Thus, it may be expected that even when the dPS block is tethered to the substrate, there will be some gain for the system by replacing some PMA segments at the air surface with dPS segments. Figure 6 shows the specular NR curves for dPS5-PMA2, for which χN has a value of about 9.5 and dPS14-PMA3, for which $\chi N = 20.5$. The data from both samples have been modeled using the same sort of two layer lamellar model used for the PMA-*b*-dPS brushes. The thicknesses of the oxide and the initiator layer were the same as used to fit the data from the PMA-*b*-dPS series. Both data sets were fit with values of the normalized sum of squared errors of less than 0.5. The SLD depth profile for dPS5-PMA2 is given in the inset of Figure 6. The final SLD profile does not exhibit two well-defined layers, and exhibits an interface between the polymer layers of large width. As with the thinnest PMA-*b*-dPS brush, the thinnest dPS-*b*-PMA brush contains chains that would probably not be ordered if they were not tethered. The important difference between the SLD profiles found for the brushes with dPS on the bottom and those with PMA on the bottom is that the width is larger for the dPS-*b*-PMA samples. Although dPS5-PMA2 has a more nearly symmetric composition ($f_{PS} = 0.52$) than does PMA2-dPS4 ($f_{PS} = 0.71$) and block lengths similar to those in PMA2-dPS4, the interface width in dPS5-PMA2 is twice as large (Table 4). The affinities of the dPS block for the air surface and PMA block for the substrate interface causes greater mixing than in the case of PMA-*b*-dPS samples. dPS5-PMA2 has an interface width of 4.2 nm and 60% of the film is composed of polymer/polymer interface. The experimental interface widths are compared in Table 4 with estimates from theory of immiscible homopolymer blends.[31]

Of the six samples from the dPS-*b*-PMA series listed in Table 2, the last four samples could not be fit using a two layer model; instead, a three-layer model had to be used. The additional layer is located at the center of the film. The NR

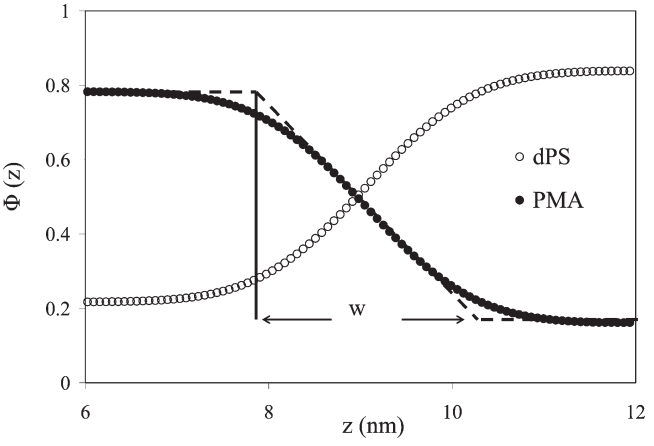

Figure 5. Compositions of dPS (open circles) and PMA (filled circles), expressed as volume fractions as a function of depth in the region of the internal interface, for PMA6-*b*-dPS5 sample. The curves were derived from the SLD plot of Figure 3. A depth of zero corresponds to the beginning of the SiO_x layer.

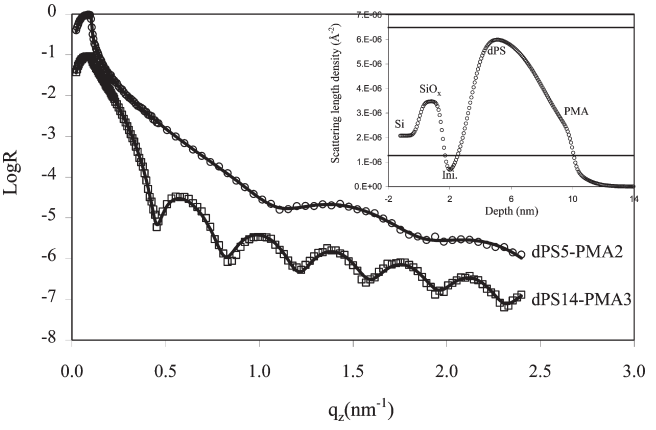

Figure 6. Neutron specular reflectivity (open symbols) and best fit model curves as a function of q_z for the two dPS-*b*-PMA brushes indicated, fit using a two-layer lamellar model. The lower curve has been shifted vertically by an order of magnitude for clarity. The inset shows the calculated SLD profile for dPS5-PMA2 as an example. The upper bold line represents the calculated SLD value expected for bulk, pure dPS and the lower bold line is that for bulk, pure PMA.

Table 4. Comparison of Theoretical and Experimental Interface Widths

sample	w_{exp1} (nm)[a]	w_{exp2}[a,b] (nm)	w_H (nm)	$w_{H,f}$ (nm)	$(d/R_g)^2/\chi N_{DCB}$	$(d/R_g)^2/\chi N_{PMA}$[c]	$(d/R_g)^2/\chi N_{dPS}$[c]
PMA2-dPS4	2.2 ± 0.4		1.8	2.4	0.77	**0.99**	0.69
PMA6-dPS5	2.4 ± 0.8		1.8	2.6	1.18	**1.28**	1.07
PMA7-dPS2	3.3 ± 1		1.8	2.6	1.26	**1.75**	0.54
PMA8-dPS2	2.0 ± 0.5		1.8	2.6	1	**1.2**	0.54
dPS5-PMA2	4.2 ± 0.5		1.8	2.5	0.65	0.21	**1.36**
dPS14-PMA3	8.4 ± 1.4		1.8	2.7	0.84	0.22	**1.32**
dPS15-PMA4	4.2 ± 1.9	5.5 ± 1.2	1.8	2.8	0.76	0.17	**1.51**
dPS15-PMA6	5.8 ± 1.8	6.6 ± 1	1.8	2.8	0.65	0.39	**0.83**
dPS11-PMA8	4.9 ± 1.4	5.4 ± 2.5	1.8	2.8	0.74	0.42	**1.28**
dPS14-PMA9	5.5 ± 2.8	4 ± 0.8	1.8	2.8	0.55	0.4	**0.7**

[a] Uncertainties represent ± 1 "standard deviation". [b] For the samples fitted by three layer model there are two polymer/polymer interfaces. w_{exp1} stands for the interface between the bottom and middle polymer layer and w_{exp2} stands for the interface between middle and top polymer layers. [c] Stretch ratios of bottom blocks are bold.

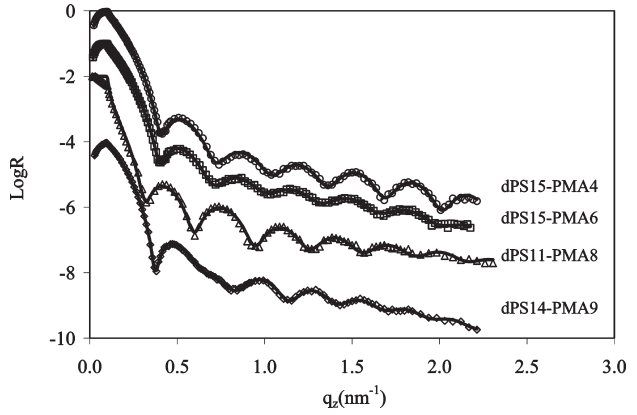

Figure 7. Neutron specular reflectivity data (open symbols) and best fit model curves (solid curves) as a function of q_z for a series of dPS-*b*-PMA brushes fit using three-layer lamellar models. Adjacent curves have been shifted vertically by an arbitrary amount for clarity.

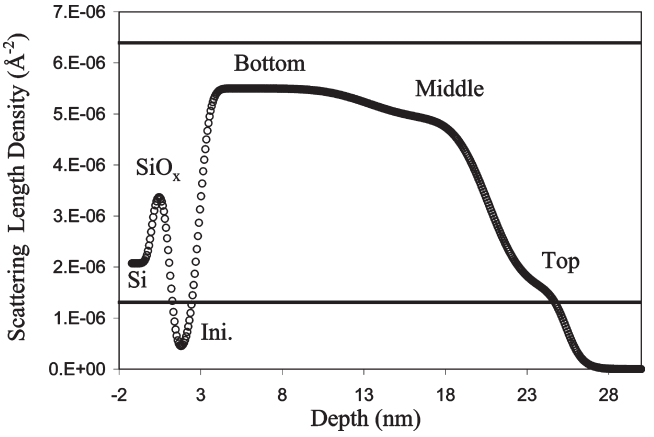

Figure 8. SLD as a function of depth for the dPS14-PMA9 sample, for which the data have been fit using a three-layer model. The bottom layer is 10 nm thick, the middle layer is 8 nm thick, and the top layer is 5 nm thick. The upper bold line represents the calculated SLD value expected for bulk, pure dPS and the lower bold line is that for bulk, pure PMA.

curves for these samples and the corresponding fits using three-layer models are given in Figure 7. The calculated SLD profile for dPS14-PMA9 is shown in Figure 8 and the depth-composition profile is given in Figure 9. The thicknesses for the oxide and initiator layers are the same as used with samples for which the two-layer model worked. The SLD of the additional layer lies between the SLD values of the dPS rich layer and PMA-rich layer and closer to the value of dPS rich layer. There is no clear trend that shows how the SLD of the additional layer varies with thickness and composition. The SLD value for the dPS-rich layer next to the substrate is similar to that seen for the two-layer models. The thicknesses obtained from NR are 10, 8, and 5 nm for the bottom, middle, and top "layers" for the dPS14-PMA9 sample (Figure 8).

The GISAXS data set from each of these samples contained weak correlation peaks at nonzero values of q_y, indicating that the structure within the brush was not uniform in the plane of the sample. The lateral correlation lengths of the in-plane structures were determined from the widths of the peaks using the Debye−Scherrer relation $\xi = 2\pi/\Delta q_y$, where Δq_y corresponds to the full width at half-maximum. The value of ξ varies from 17 to 20 nm for these four samples. The position of the correlation peak gives the domain−domain distance of the in-plane structure and this spacing varies from 10 to 14 nm. Thus, the ordering is limited

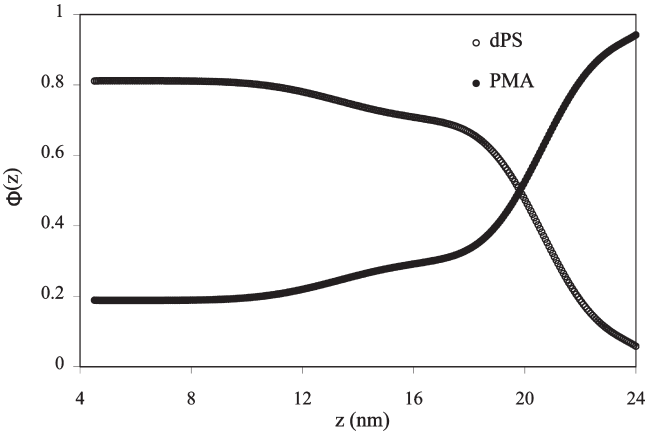

Figure 9. Compositions of dPS (open circles) and PMA (filled circles), expressed as volume fractions as a function of depth in the region of the internal interface, for the dPS14-PMA9 sample. The curves were derived from the SLD plot of Figure 8. A depth of zero corresponds to the beginning of the SiO_x layer.

to nearest neighbor correlation; there is no long-range ordering. Specular NR cannot resolve the lateral variations in SLD corresponding to this structure, but it is sensitive to the laterally average structure. One feature of this laterally separated structure that the NR analysis gives us is the height of the laterally separated domains in the middle of the film. These appear not to extend through the entire thickness of the brush, but rather the NR data indicate that there is a laterally uniform layer at the air surface and at the substrate interface.

Scaling and Self-Consistent Field (SCF) Theory for Interfacial Widths in DCBs. To explain the interfacial widths observed experimentally, we present here a scaling theory and SCF calculations for the interfacial width in a DCB. To better understand the dominant forces determining the width in a DCB, we first review the cases of an immiscible blend and a free diblock copolymer.

The width of an interface between immiscible blocks has been well studied in both blends of homopolymers as well as block copolymers. Experiments have shown that the observed widths are fairly diffuse,[9b,32] and when the effect of interfacial fluctuations are taken into account generally agree with the predictions of the Helfand−Tagami theory,[29,31] which uses a SCF calculation to derive an expression for the interfacial width

$$w_H = \frac{2b}{\sqrt{6\chi}} \tag{4}$$

for the case of infinite molecular weight polymers ($N \rightarrow \infty$), in terms of the statistical segment length, b, and Flory interaction parameter, χ, between monomers of type A and type B. The proportionalities in this relationship for a blend of immiscible homopolymers can be understood using a simple scaling argument[33] in which the width is determined by a balance of chain conformational entropy and the free energy of mixing. Namely, the interfacial region is spanned by an excursion of one chain, that is, a "blob", say composed of N_w type-A monomers, into the region rich in type-B monomers. These fluctuations will have energy of order k_BT. Because the energetic penalty of having N_w type-A monomers in a B-rich region scales as $N_w\chi k_BT$, this implies $N_w \approx 1/\chi$. Inside this blob, because the interaction energy is less than k_BT, the conformations can be considered to be Gaussian and, thus, the size of this excursion is $w \approx \sqrt{N_w}b \approx b/\sqrt{\chi}$, which is consistent with the Helfand expression up to prefactors. Furthermore,

because each blob corresponds to an excess of energy on the order of k_BT and occupies area $N_w/(\rho w)$, where ρ is the monomer density, the surface tension scaling is given by the ratio of the two, $\gamma \approx k_BT\rho\omega/N_w \approx k_BT\chi\rho\omega$. Substituting for the width gives $\gamma \approx \rho b\sqrt{\chi}k_BT$, which likewise agrees up to prefactors with the Helfand−Tagami expression[31]

$$\gamma \approx \rho b\sqrt{\chi/6}k_BT \tag{5}$$

for polymers having (nearly) equal statistical segment lengths.

Eq 4, using a value of averaged statistical segment length, b, of 0.71 nm appropriate for PMA and dPS, yields a value for w_H of 1.83 nm. This value is smaller than the experimentally measured w_{exp} values in this work. This is to be expected, not only due to the difference between immiscible homopolymer interfaces and bulk and grafted diblock copolymer interfaces but also because interface fluctuations due to capillary waves have been ignored in the Helfand−Tagami calculation. The effective interface width measured by NR represents a convolution of the intrinsic width and a broadening due to fluctuations[34−36] in the position of the nominal interface. A proper comparison must account for these fluctuations. For untethered chains, the mean-square displacement of the interface from its average position, $\langle(\Delta z)^2\rangle$, is given by[34]

$$\langle(\Delta z)^2\rangle = k_BT\ln(\lambda_{max}/\lambda_{min})/2\pi\gamma_{AB} \tag{6}$$

where λ_{min} and λ_{max} are the minimum and maximum wavelengths of the fluctuations, and γ_{AB} is the interfacial tension between immiscible homopolymers. Using the value of b = 0.71 nm and a value of $1/\rho_0 = 137$ Å^3, we obtain an estimate of 2.75 dyn/cm for the interfacial tension between PS and PMA homopolymers at 25 °C. To estimate the values of λ_{max} and λ_{min} we turn to the theoretical work of Fredrickson and co-workers[24] on surface fluctuations in grafted brushes. They argued that surface fluctuations (which are Rayleigh waves) with wavelengths greater than the film thickness are strongly suppressed due to the cost of chain stretching. Very short wavelength modes are also suppressed due to the action of surface tension. Thus, there is a preferred fluctuation wavelength that should be on the order of equilibrium brush height. We take λ_{max} to be the total brush thickness, which varies from 6 to 11 nm for samples in the PMA-*b*-dPS series or 7 to 23 nm for samples in the dPS-*b*-PMA series. The value of λ_{min} is expected to be close to the intrinsic interface width and we adopt a value of 1 nm. With these assumptions we find $\langle(\Delta z)^2\rangle^{1/2} \approx 0.8$ nm. Convolution of a Gaussian distribution of interface positions with a step function profile gives an error function profile with an interface width, w_{fluc}, of $\langle 2\pi(\Delta z)^2\rangle^{1/2}$. Thus, the interface width ascribed to interface fluctuations is about 2 nm. The overall interface width, $w_{H,f}$, is then predicted to be

$$w_{H,f}{}^2 = w_H{}^2 + w_{fluc}{}^2 \tag{7}$$

which is listed in Table 4 for all the samples.

For the case of dry bulk diblock copolymers, in principle one needs to consider the possibility that chain stretching may affect the interfacial width, since the tendency toward microphase separation acts to stretch the polymer chains away from the interface. Indeed, in the strong-stretching limit, each block of a polymer chain can be considered as effectively tethered to the interface, similar to a brush. The degree of stretching, or equivalently, the areal density of chains at the interface, is given then by a competition between the free energy of the stretched chain, favoring shorter chains, and the interfacial free energy, favoring longer chains, which occupy less area. This balance leads to a chain extension, corresponding to the microphase domain spacing

$$d \approx \left(\frac{\gamma b^2N^2}{\rho k_BT}\right)^{1/3} \tag{8}$$

where γ is an interfacial tension between the two domains and N is the number of monomers in a block.[33] Because $d/\sigma = N/\rho$, this is equivalent to an areal density of chains

$$\sigma = \left(\frac{\gamma b^2\rho^2}{Nk_BT}\right)^{1/3} \tag{9}$$

Despite the potential for chain stretching to play a role, the interfacial widths in bulk untethered block copolymers predicted by the same SCF approach and observed experimentally are only slightly larger, or nearly the same for large χN ($\chi N \geq 20$), as the Helfand−Tagami expressions above for a blend of immiscible homopolymers.[29,31] We will see below that this is a result of the fact that a system of free diblock copolymers adjusts its interfacial areal chain density to minimize free energy, and in so doing, the portion of a chain spanning the width of the interface always has stretching energy less than k_BT and is, thus, largely unaffected in size by the chain stretching.

Stretched Interface Scaling Regime. Turning now to the case at hand of the internal interface of a dry DCB, one sees that a key difference with the free block copolymer is that the grafting density is fixed, and the free energy cost of stretching cannot be compensated by an areal dilution of chains. As a result, a block copolymer can be in a state of greater stretching when grafted compared to when it is untethered. The size ξ of a tension blob, that is, the length of chain for which the stretching energy is on the order of k_BT, is given by $\xi \approx (g^{1/2})b$. The number of monomers in the tension blob, g, is given by the relation $(N/g)\xi \approx d$ expressing the fact that on scales larger than ξ, the chain conformation is stretched into a line of tension blobs,[37] giving

$$g \approx \left(\frac{Nb}{d}\right)^2 \approx \left(\frac{\rho b}{\sigma}\right)^2 \approx N/\left(\frac{d}{R_g}\right)^2 \tag{10}$$

and

$$\xi \approx \frac{Nb^2}{d} \approx \frac{\rho b^2}{\sigma} \approx \left(\frac{R_g}{d}\right)R_g \tag{11}$$

The interface still consists of fluctuations of the monomers of one block into the other, and we might expect that these excursions are not strongly dependent on the tension in the polymer, particularly in the limit of long chains. Then, as before, we expect that the number of such monomers is $N_w \approx 1/\chi$. This therefore leads to two scaling regimes: (*i*) $N_w < g$, for which the monomers in the interface are unstretched, corresponding to the conventional Helfand−Tagami regime with $w \approx b/(\chi^{1/2})$, and (*ii*) $N_w > g$, for which the portions of a chain in the interface exceed a tension blob and thus assume a stretched conformation, corresponding to a new *stretched interface* regime. In this stretched interface regime, the interfacial width is given by

$$w \approx \left(\frac{N_w}{g}\right)\xi \approx \left(\frac{N_w}{N}\right)d \approx \frac{d}{\chi N} \approx \frac{\sigma}{\chi\rho} \tag{12}$$

In contrast to the Helfand regime, where the interfacial width scales as $\chi^{-1/2}$ and is independent of areal chain

density, in the stretched interface regime the interfacial width scales as χ^{-1} and is proportional to the areal chain (grafting) density, σ. Note that the independence from molecular weight is maintained because $d \propto N$. However, the threshold for crossing over into the stretched interface regime can be expressed as

$$N_w > g \quad \text{or} \quad w > \xi \quad \text{or} \quad (d/R_g)^2 > \chi N \quad \text{or} \quad \left(\frac{\sigma}{\rho b}\right)^2 > \chi$$

For example, the interface is expected to be stretched when the square of the ratio of brush height to R_g is large compared to χN. We see that larger grafting densities favor stretching, whereas larger χ values favor narrow interfaces that eventually are narrow enough that the stretching energy of chains there can be neglected. These results are summarized in Figure 10.

This analysis allows us to see why the stretched interface regime is not normally accessible in free block copolymer systems, but is instead limited to DCBs. For a free block copolymer to enter the stretched interface regime, the grafting density would have to satisfy $(\sigma/\rho b)^2 > \chi$. Using the expression above for σ in free diblocks and $\gamma \approx \rho b(\chi^{1/2})k_B T$ for the interfacial tension, we find that the criterion for stretched interfaces in free block copolymers reduces to $\chi N < 1$. This is incompatible with the significantly higher values of $\chi N > 10$ needed for microphase separation, and thus, when microphase separation is seen, the interfaces will be in the Helfand regime.

We tested these scaling ideas against SCF calculations of DCBs with varying brush parameters. The DCB interaction free energy was modeled as

$$W[\rho_A(z), \rho_B(z)]/k_B T = \int \frac{1}{2} v[\rho_A(z) + \rho_B(z) - \rho]^2 + \chi \rho_A(z)\rho_B(z) d\mathbf{r} \quad (13)$$

with v, an adjustable compressibility parameter, and the intrinsic conformations of the diblock chains taken to be Gaussian. This leads to a self-consistent solution for the density field for A-monomers

$$\rho_A(z) = \sigma \frac{\int_0^{fN} dt q(z;t) q^\dagger(z;t)}{\int dz q(z;N) q^\dagger(z;N)} \quad (14)$$

and similarly for $\rho_B(Z)$, where f is the fraction of monomers, which are A-type. The reduced propagators $q(z;t)$ and $q^\dagger(z;t)$, starting from the grafted chain end and the free end, respectively, satisfy the modified diffusion equations

$$\frac{\partial q(z;t)}{\partial t} = \frac{b^2}{6}\frac{\partial^2 q(z;t)}{\partial z^2} - \mu(z;t) q(z;t),$$
$$\mu(z;t) = \begin{cases} \mu_A(z) & 0 \le t \le fN \\ \mu_B(z) & fN \le t \le N \end{cases} \quad (15)$$

in the chemical potential fields $\mu_K(z) = \delta W/\delta \rho_K(z)$, with $K =$ A or B. The grafting condition at one end only is enforced by the initial conditions $q(z = 0;t = 0) = 1$, $q(z \neq 0;t = 0) = 0$ and $q^\dagger(z;N) = 1$, and the boundary conditions $q(z < 0;t) = q^\dagger(z < 0;t) = 0$ and $q(z > L;t) = q^\dagger(z > L;t) = 0$ define a box with walls at $z = 0$ and $z = L$. To mimic the effects of cohesion in a dry brush, the box length L was taken to be the expected height d of a brush having a density equal to that of a melt, with a compressibility parameter v taken large enough that the density profile is fairly flat. A separate comparison was done with a strictly incompressible SCF theory that produced consistent results. Details of the calculation method can be found in elsewhere.[8]

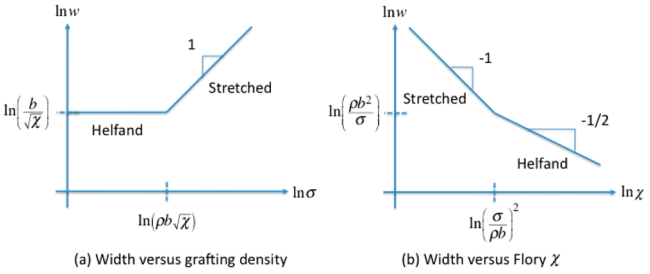

Figure 10. Scaling of interfacial width w vs (a) grafting density σ and (b) Flory χ parameter, showing crossover from Helfand regime to stretched interface regime.

Figure 11 shows the SCF results for the interfacial width versus grafting density, Flory χ parameter, and number of monomers. Overall, there is quite good agreement with the predictions of the scaling theory, which neglects variations in chain extension both between chains and along a single chain. The width shows a clear crossover from grafting density independence in the Helfand regime to a width that increases with grafting density. Likewise, the dependence on the Flory χ parameter shows a break between two slopes, which are close to the predicted scaling slopes of -1 and $-1/2$. Finally, as expected according to the scaling theory, there is negligible dependence on the molecular weight throughout both Helfand and stretched interface regimes.

Comparison between Experiment and Theory. To make comparison with theory, we will estimate stretch ratios of $(d/R_g)^2$ to χN to determine which brush samples may be close to or in the stretched interface regime. From the SCF calculations and within uncertainties, we would expect the crossover to the stretched interface regime to occur at values of stretch ratio around 0.2−2. As mentioned above, the relative stretching is nonuniform in a brush and tends to be stronger near the grafting point than near the free end, and so Table 4 lists values of this ratio for each block as well as for the brush taken as a whole. The stretch ratio of the grafted block (0.7−1.75) clearly shows stronger stretching than in the free block (0.17−1.07), while the range for the brush taken as a whole was from 0.55 to 1.26, with the largest values occurring for the samples PMA7-dPS2 and PMA6-dPS5. For each sample, the experimentally measured interface widths are listed along with, as a reference, the Helfand widths and Helfand widths corrected for interfacial fluctuations in Table 4.

Of the four brushes with grafted PMA blocks, the two samples with the largest stretch ratio do in fact show the greatest ratio of experimental widths to the Helfand widths corrected for capillary fluctuations, as shown in Figure 12. Of the samples with grafted dPS blocks, it should be noted that only dPS5-PMA2 and dPS14-PMA3 were well described by a single interface, with the interface width for dPS14-PMA3 being strikingly large. (As discussed below, the remaining samples have more complicated structures that are three-dimensional.) With the samples for which dPS is grafted to the substrate, it is more difficult to establish a trend, because there are only two points. However, we can make two observations. First, the ratios of experimental to theoretical interface widths for these samples are much higher than for the samples in which the PMA block is grafted. Second, this ratio of experimental to theoretical width does increase with stretch ratio, and much more sharply than for the brushes with PMA grafted to the substrate. We conjecture that the sequence of blocks in the chain is extremely

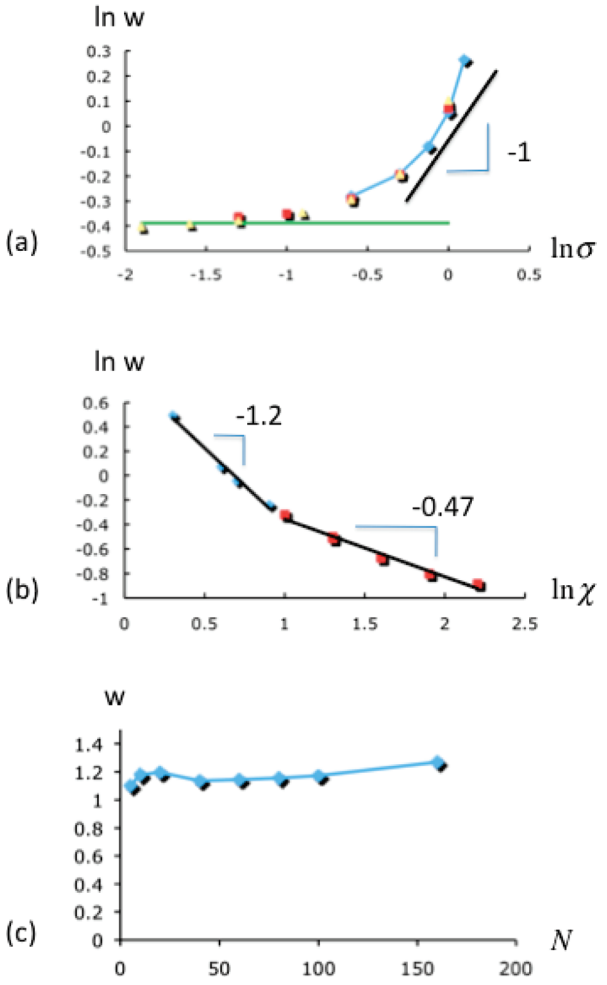

Figure 11. Results of SCF calculations for the interfacial width, w, vs (a) grafting density σ ($\chi = 4$, $N = 40$ blue diamonds, $N = 100$ red squares, $N = 160$ yellow triangles); (b) Flory χ parameter ($\sigma = 1$, $N = 10$); and (c) number of monomers N ($\sigma = 1$, $\chi = 4$). The lines in (a) are the expected slopes from scaling; the lines in (b) are best linear fits whose slopes are displayed. The unit of length in these plots is taken to be b.

important. Because the dPS block is preferred at the surface the block sequence in PMA-dPS samples leads more readily to well-defined lamellar structures. In dPS-PMA samples the drive to place dPS segments at the surface leads to much broader interfaces.

While the calculated Helfand interface widths corrected for fluctuations, $w_{H,f}$, are generally in the same range as experimental values of w for the PMA-*b*-dPS series, they are noticeably lower than experiment for the dPS-*b*-PMA series. Because the dPS blocks are attached to the substrate, but dPS is enthalpically preferred at the air surface, the two blocks mix more than they would otherwise, broadening the interface. The cost for dPS chains to stretch away from the tethering sites is compensated by the reduction in surface tension accomplished by putting dPS segments at the surface. A possible contributing factor toward explaining the discrepancy between the experimental and the theoretical w values is that the theoretical calculations do not take into account the existence of additional interfaces on either side of the interface of central interest. Details of these other interfaces have the effect of imposing additional biasing fields on the polymer chains in the brush.

Direct comparison between experiment and SCFT calculations using experimental parameters has been attempted for three samples: PMA6-dPS5, dPS5- PMA2, and dPS14-PMA9.

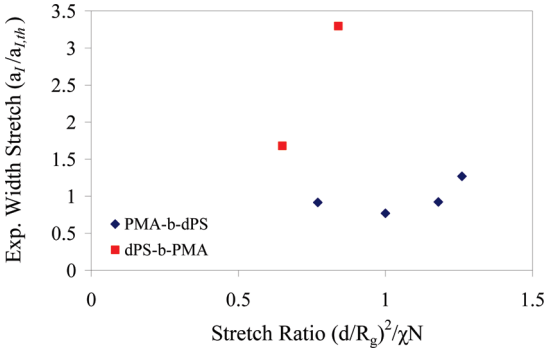

Figure 12. Plot showing positive correlation between the ratio of observed interfacial width to the Helfand width, and the stretch ratio $(d/R_g)^2/(\chi N)$ for PMA-dPS DCBs, in qualitative agreement with the scaling theory.

As explained below, two approximate methods were used to model the sharp surface of a dry brush. In the first approach, the polymer was assumed to be at the bulk density resulting from cohesive forces, and this constrains the brush height. Density fluctuations are accounted for by a compressibility factor. This was the approach taken in ref 8 and can account for tethering and additional effects at the substrate and air interfaces through the use of effective surface potentials. In the second approach, the DCB is considered to be in the presence of nonpreferential solvent. The interface width is obtained as a function of the interaction parameter between the solvent and the block copolymer. The dry brush case is taken to be the limit of poor solvent. However, because the calculation becomes more difficult as the solvent quality becomes poorer, the value of interface width for the case of the dry DCB is obtained by extrapolation. The two methods of accounting for the behavior of a dry DCB produce consistent values of the interfacial width.

Here we compare the experimentally measured values to interface widths calculated with SCFT[8] using the first approach, which accounts for the tethering at the substrate interface, but does not attempt to capture the differing affinities of the two blocks for the substrate and air interfaces. Another feature of the actual sample captured in this calculation is the existence of grafted homopolymer in the brush. We have assumed for purposes of this calculation that the DCB contains about 10% homopolymer brush[3b] having repeat units the same as those in the first block of the block copolymers. The segment density depth profiles for PMA and dPS calculated using parameters characteristic of the PMA6-dPS5 sample are shown in Figure 13. The overall grafting density has been taken as 0.8 chains/nm^2 and the grafting density of the diblock chains as 0.7 chains/nm^2 (i.e., only 7 of 8 chains of the first block synthesized are assumed to reinitiate.) The value of interface width (defined according to Helfand's convention[29]) derived from Figure 13 is 4.0 nm. The SCFT using the nonselective solvent gives an equivalent extrapolated interface width. This is larger than the experimentally observed value of 2.4 ± 0.8 nm.

In fact, the calculation is insensitive to the order in which the blocks are located in the chains, so that an interface width of 4 nm is found from an SCFT calculation also for the corresponding brush with the PS block tethered to the substrate. In the calculation it is assumed that the dPS segregates preferentially to both air and substrate interfaces. The SCFT calculations performed here, however, do not include surface energy preferences for or against PS over PMA, which may play a role in explaining the dependence of interface width on the identity of the block tethered to the

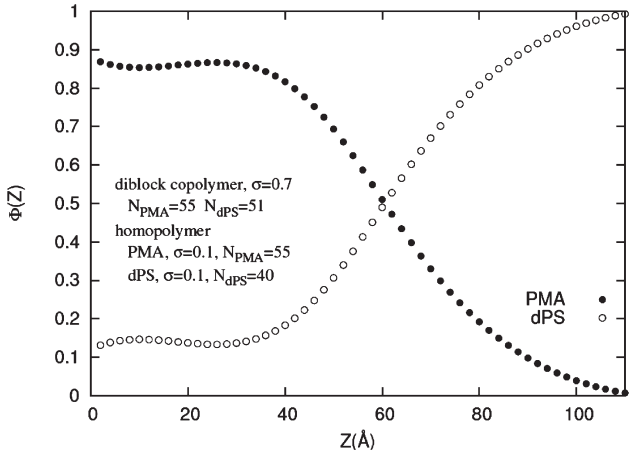

Figure 13. Segment density of PMA (filled circles) and dPS (empty circles) as a function of depth for the PMA6-dPS5 brush calculated using SCF theory. Grafting density for the diblock was taken to be 0.7 (chains/nm^2) and that for the PMA and dPS homopolymers 0.1 (chains/nm^2).

substrate. Consistent with this explanation, varying the strength of a preferential surface field added to the SCFT calculations did result in changes in the shape and apparent width of the profile (data not shown), but quantitative conclusions are limited by a lack of detailed information about the surface potential.

The interface widths found by the second SCFT method for dPS5- PMA2 and by the first SCFT method for dPS14-PMA9 are the same: 4 nm. The experimental interface width for dPS5-PMA2 (4.2 ± 0.5 nm) is consistent with the interface width obtained by SCFT. It is very difficult to make comparisons between the theory and experiment for dPS14-PMA9 because this sample has in-plane ordering. However, the interface width calculated using SCFT agrees well with the two experimental values (5.5 ± 2.8 and 4 ± 0.8 nm) obtained from NR for this sample. SCFT calculations are still in progress and we believe the SCFT results will be improved by adding differing affinities of the two blocks for the substrate and air interfaces.

The most meaningful comparisons, however, will require 3-D calculations. The SCFT described here assumes that the brush structure is laterally homogeneous. GISAXS measurements have shown, though, that the sample dPS14-PMA9 is not laterally uniform. In fact, in general the internal structure of brushes with thickness $d \geq 19$ nm cannot be described by one-dimensional models that account only for layering in the z-direction. Rather, a 3-D model of internal structure is required.

It may not be thickness that determines whether a 3-D structure is formed by the brush. For a series of brushes in which the grafting density is held constant chain length N increases with thickness. Thus, the thicker brushes are those with larger values of the parameter χN, which measures the propensity of the diblock chains to order into domains. Presumably, at low values of χN a lamellar geometry can be imposed on the ordered material by tethering to a flat substrate and the penalty against curvature imposed by the polymer/air interface, even if the composition of the chain is far from symmetric. Once χN becomes large enough (> 23), the drive to reduce contacts between unlike segments is sufficient to force the formation of curved interfaces within the brush, despite the planar geometry imposed at the top and bottom interfaces. Detailed 3-D modeling of the internal structure to explore this concept and capture the features observed in GISAXS data will be the subject of a future publication.

Conclusion

Neutron reflectometry measurements have revealed for the first time details of the internal structure of dPS-*b*-PMA and PMA-*b*-dPS DCBs. For the brushes with dPS and PMA blocks, which are characterized by a moderate block−block χ parameter, sufficiently thin brushes adopt a lamellar internal morphology even when the chain composition is quite asymmetric. This layering results from the effective biasing fields imposed by the tethering, the affinities of each block for a given interface and the van der Waals interactions of the polymers with the substrate. For brushes characterized by values of $\chi N \approx 7-22$ each layer in the lamellar structure contains a substantial volume fraction of each block. Less mixing would be expected for brushes with larger values of χN. The width of the internal interface for PMA-*b*-dPS samples is equal to that expected in an ordered bulk mesophase of an untethered analog of the brush chain, whereas it is greater for dPS-*b*-PMA samples than for untethered chains. This is due to the affinities of the two blocks for opposite interfaces and this feature was not considered by previous theories. For brushes with sufficiently high values of χN (> 23), the internal structures in the as-deposited DCBs can no longer be represented with lamellar models, but rather in-plane variations in the composition must be considered.

Consideration of a scaling theory for the interface width in DCBs provides some insights. Specifically, it identifies two regimes in the dependence of interface width on grafting density and on χ. For lower grafting density, interface width is weakly dependent on σ. When σ is sufficiently high to cause strong stretching, the interface width increases markedly with grafting density. When χ is small, the interface width varies as χ^{-1}. For large χ, the exponent is about -0.5, as anticipated by Helfand. Interface width is mostly independent of N. Comparisons show qualitative consistency between the experimental trends in interface width and those predicted by a scaling theory, but a more rigorous validation would require further careful measurements. A particular characterization challenge is the unambiguous identification of the grafting density. This issue is further complicated by the possibility that polymerization of some of the second block is initiated on the grafting surface while attempting to grow it from the living ends of the first block. Moreover, there is currently a limited range for the control of grafting density. An alternate route to test the stretched interface regime is to use blocks with smaller values of χ. Larger values of χ will also aid in mapping out the crossover from the classical Helfand regime to the stretched interface regime.

SCFT calculation of the interface width for a sample with PMA tethered to the substrate estimates an interface width larger than the experimental width, while an analogous calculation for a sample with the dPS block tethered to the substrate agrees well with experiment for dPS5-PMA2.

Acknowledgment. The authors gratefully thank Prof. Scott Collins for the use of his drybox. Use of the Advanced Photon Source was supported by the U.S. Department of Energy, Office of Science, Office of Basic Energy Science, under Contract No. W-31-109-ENG-38. Technical support by sector 8 staff at the APS is gratefully acknowledged. Acknowledgment is made to the donors of The American Chemical Society Petroleum Research Fund for partial support of this research (AC7-42995). Partial support from an Ohio Board of Regents challenge grant is gratefully acknowledged. D.T.W. also acknowledges partial support from NSF Award # DMR-0213918 and AFOSR Award # FA9550-08-1-0007.

Note Added after ASAP Publication. This article was published ASAP on September 23, 2009. Several equations in

the Results and Discussion section have been modified. The corrected version was published on September 25, 2009.

Supporting Information Available: Contact angle and ATR-IR characterizations of diblock copolymer brushes. This material is available free of charge via the Internet at http://pubs.acs.org.

References and Notes

(1) (a) Zhao, B.; Brittain, W. J.; Zhou, W.; Cheng, S. Z. D. *J. Am. Chem. Soc.* **2000**, *122*, 2407. (b) Minko, S. *Polym. Rev.* **2006**, *46*, 397. (c) Xiong, H.; Zheng, J. X.; Van Horn, R. M.; Jeong, K.; Quirk, R. P.; Lotz, B.; Thomas, E. L.; Brittain, W. J.; Cheng, S. Z. D. *Polymer* **2007**, *48*, 3732. (d) Rowe, M. D.; Hammer, B. A. G.; Boyes, S. G. *Macromolecules* **2008**, *41*, 4147. (e) Gao, X.; Feng, W.; Zhu, S.; Sheardown, H.; Brash, J. L. *Langmuir* **2008**, *24*, 8303. (f) Yamamoto, S.-I.; Pietrasik, J.; Matyjaszewski, K. *Macromolecules* **2008**, *41*, 7013. (g) Tomlinson, M. R.; Genzer, J. *Polymer* **2008**, *49*, 4837.

(2) (a) Zhao, B.; Brittain, W. J. *Macromolecules* **2000**, *33*, 8813. (b) Zhao, B.; Brittain, W. J.; Zhou, W.; Cheng, S. Z. D. *Macromolecules* **2000**, *33*, 8821. (c) Sedjo, R. A.; Mirous, B. K.; Brittain, W. J. *Macromolecules* **2000**, *33*, 1492. (d) Baum, M.; Brittain, W. J. *Macromolecules* **2002**, *35*, 610. (e) Tomlinson, M. R.; Genzer, J. *Chem. Commun.* **2003**, *12*, 1350. (f) Granville, A. M.; Boyes, S. G.; Akgun, B.; Foster, M. D.; Brittain, W. J. *Macromolecules* **2004**, *37*, 2790. (g) Granville, A. M.; Boyes, S. G.; Akgun, B.; Foster, M. D.; Brittain, W. J. *Macromolecules* **2005**, *38*, 3263. (h) Xu, C.; Wu, T.; Drain, C. M.; Batteas, J. D.; Fasolka, M. J.; Beers, K. L. *Macromolecules* **2006**, *39*, 3359.

(3) (a) Boyes, S. G.; Brittain, W. J.; Weng, X.; Cheng, S. Z. D. *Macromolecules* **2002**, *35*, 4960. (b) Kim, J.-B.; Huang, W.; Bruening, M. L.; Baker, G. L. *Macromolecules* **2002**, *35*, 5410. (c) Huang, W.; Kim, J.-B.; Baker, G. L.; Bruening, M. L. *Nanotechnology* **2003**, *14*, 1075.

(4) (a) Gersappe, D.; Fasolka, M.; Israels, R.; Balazs, A. C. *Macromolecules* **1995**, *28*, 4753. (b) Yin, Y.; Sun, P.; Li, B.; Chen, T.; Jin, Q.; Ding, D.; Shi, A.-C. *Macromolecules* **2007**, *40*, 5161. (c) Meng, D.; Wang, Q. *J. Chem. Phys.* **2009**, *130*, 134904.

(5) Zhulina, E. B.; Singh, C.; Balazs, A. C. *Macromolecules* **1996**, *29*, 6338.

(6) Zhulina, E. B.; Singh, C.; Balazs, A. C. *Macromolecules* **1996**, *29*, 8254.

(7) Ferreira, P. G.; Leibler, L. *J. Chem. Phys.* **1996**, *105*, 9362.

(8) Heine, D.; Wu, D. T. *J. Chem. Phys.* **2001**, *114*, 5313.

(9) (a) Russell, T. P. *Mater. Sci. Rep.* **1990**, *5*, 171. (b) Anastasiadis, S. H.; Russell, T. P.; Satija, S. K.; Majkrzak, C. F. *J. Chem. Phys.* **1990**, *92*, 5677. (c) Foster, M. D.; Sikka, M.; Singh, N.; Bates, F. S.; Satija, S. K.; Majkrzak, C. F. *J. Chem. Phys.* **1992**, *96*, 8605.

(10) Commercial materials, instruments, and equipment are identified in this paper to specify the experimental procedure as completely as possible. In no case does such identification imply a recommendation or endorsement by the National Institute of Standards and Technology nor does it imply that the materials, instruments, or equipment identified are necessarily the best available for the purpose.

(11) Keller, R. N.; Wycoff, H. D. *Inorg. Synth.* **1946**, *2*, 1.

(12) Piranha etching consists of using hydrogen peroxide and sulfuric acid, which can be dangerous. Acid-resistant gloves, protective goggles, and lab coats must be worn when handling the piranha solution.

(13) Matjyaszewski, K.; Miller, P. J.; Shukla, N.; Immaraporn, B.; Gelman, A.; Luokala, B. B.; Siclovan, T. M.; Kickelbick, G.; Vallant, T.; Hoffmann, H.; Pakula, T. *Macromolecules* **1999**, *32*, 8716.

(14) (a) Hamilton, W. A. *Curr. Opin. Colloid Interface Sci.* **2005**, *9*, 390. (b) Lin, Y.; Böker, A.; He, J.; Sill, K.; Xiang, H.; Abetz, C.; Li, X.; Wang, J.; Emrick, T.; Long, S.; Wang, Q; Balazs, A.; Russell, T. P. *Nature* **2005**, *434*, 55. (c) Papadakis, C. M.; Busch, P.; Posselt, D.; Smilgies, D. M. *Adv. Solid State Phys* **2004**, *44*, 327. (d) Lee, B.; Park, I.; Yoon, J.; Park, S.; Kim, J.; Kim, K.; Chang, T.; Ree, M. *Macromolecules* **2005**, *38*, 4311. (e) Muller-Buschbaum, P.; Hermsdorf, N.; Roth, S. V.; Wiedersich, J.; Cunis, S.; Gehrke, R. *Spectrochim. Acta, Part B* **2004**, *59*, 1789.

(15) Foster, M. D. *Crit. Rev. Anal. Chem.* **1993**, *24*, 179.

(16) Haaland, P.; Targove, J. *Appl. Phys. Lett.* **1992**, *61*, 34.

(17) Parratt, L. G. *Phys. Rev.* **1954**, *95*, 359.

(18) Xia, J.; Matjyaszewski, K. *Macromolecules* **1997**, *30*, 7697.

(19) (a) Tsujii, Y.; Ejaz, M.; Yamamoto, S.; Fukuda, T.; Shigeto, K.; Mibu, K.; Shinjo, T. *Polymer* **2002**, *43*, 3837. (b) von Werne, T.; Patten, T. E. *J. Am. Chem. Soc.* **2001**, *123*, 7497.

(20) Husseman, M.; Malmstrom, E. E.; McNamara, M.; Mate, M.; Mecerreyes, O.; Benoit, D. G.; Hedrick, J. L.; Mansky, P.; Huang, E.; Russell, T. P.; Hawker, C. J. *Macromolecules* **1999**, *32*, 1424.

(21) van Krevelen, D. W. *Properties of Polymers: Their Correlation with Chemical Structure, Their Numerical Estimation and Prediction from Additive Group Contributions*; Elsevier Science: Amsterdam, 1990; p 202.

(22) Russell, T. P.; Hjelm, R. P.; Seeger, P. *Macromolecules* **1990**, *23*, 890.

(23) Hashimoto, T.; Shibayama, M.; Kawai, H. *Macromolecules* **1980**, *13*, 1237.

(24) Fredrickson, G. H.; Ajdari, A.; Leibler, L.; Carton, J.-P. *Macromolecules* **1992**, *25*, 2882.

(25) Akgun, B.; Uğur, G.; Zhang, J.; Narayanan, S.; Song, S.; Lee, H.; Brittain, W. J.; Kim, H.; Sinha, S. K.; Foster, M. D. *Macromolecules* **2009**, *42*, 737.

(26) Akgun, B.; Brittain, W. J.; Li, X.; Wang, J.; Foster, M. D. *Macromolecules* **2005**, *38*, 8614.

(27) Kim, J.-B.; Bruening, M. L.; Baker, G. L. *J. Am. Chem. Soc.* **2000**, *122*, 7616.

(28) Brittain, W. J.; Boyes, S. G.; Granville, A. M.; Baum, M.; Mirous, B. K.; Akgun, B., Zhao, B.; Blickle, C.; Foster, M. D. Surface Rearrangement of Diblock Copolymer Brushes-Stimuli Responsive Films. In *Surface-Initiated Polymerization II; Adv. Polym. Sci. 198*; Jordan, R., Ed.; Springer: Berlin/Heidelberg, 2006; pp 125−147.

(29) Helfand, E.; Wasserman, Z. R. *Macromolecules* **1976**, *9*, 879.

(30) *Polymer Handbook*; Brandrup, J., Immergut, E. H., Grulke, E. A., Eds., Wiley & Sons: New York, 1999.

(31) (a) Helfand, E.; Tagami, Y. *J. Chem. Phys.* **1971**, *56*, 3592. (b) Helfand, E.; Sapse, A. M. *J. Chem. Phys.* **1975**, *62*, 1327.

(32) (a) Fernandez, M. L.; Higgins, J. S.; Penfold, J.; Ward, R. C.; Shockleton, C.; Walsh, D. J. *Polymer* **1988**, *29*, 1923. (b) Schubert, D. W.; Stamm, M. *Europhys. Lett.* **1996**, *35*, 419.

(33) Milner, S. T. *Science* **1991**, *251*, 905.

(34) Shull, K. R.; Mayes, A. M.; Russell, T. P. *Macromolecules* **1993**, *26*, 3929.

(35) Buff, F. P.; Lowett, R. A.; Stillinger, F. H. *Phys. Rev. Lett.* **1965**, *15*, 621.

(36) Rowlinson, J.; Widom, B. *Molecular Theory of Capillarity*; Oxford University Press: Oxford, U.K., 1982.

(37) Dobrynin, A. V.; Colby, R. H.; Rubinstein, M. *Macromolecules* **1995**, *28*, 1859.